Radial Sizing of Lipid Nanotubes Using Membrane Displacement Analysis

Natalia Stepanyants, Gavin D. M. Jeffries, Owe Orwar, and Aldo Jesorka*

Department of Chemical and Biological Engineering, Chalmers University of Technology, SE-41296 Göteborg, Sweden

S *Supporting Information*

ABSTRACT: We report a novel method for the measurement of lipid nanotube radii. Membrane translocation is monitored between two nanotube-connected vesicles, during the expansion of a receiving vesicle, by observing a photobleached region of the nanotube. We elucidate nanotube radii, extracted from SPE vesicles, enabling quantification of membrane composition and lamellarity. Variances of nanotube radii were measured, showing a growth of 40−56 nm, upon increasing cholesterol content from 0 to 20%.

KEYWORDS: *Lipid nanotube, membrane displacement, vesicle, cholesterol*
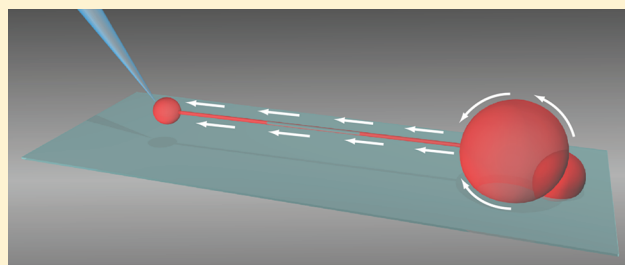
Lipid nanotubes have been found to play important roles in both intracellular processes[1,2] and intercellular communication pathways.[3,4] Recent studies have investigated their influence on immunological responses,[5−7] pathogen transfer,[8−12] and chemical signaling[13] as well as formation mechanisms.[4,14,15]

Various nanotube vesicle network geometries have been generated *in vitro*, and employed as models for these lipid structures, to better understand membrane shape transformations, transport phenomena, and chemistry within confined environments.[16] Transport of species through the nanotubes, as well as tension-driven membrane material transfer along the nanotubes,[16] has been investigated, expanding the model for transport of membrane and cytoplasmic components between cells.[3]

Nanotube radii have been estimated to be within the range 10−150 nm.[17−19] As lipid nanotubes are significantly below the resolution limit of optical microscopy,[20] accurate sizing determination has, thus far, proven extremely challenging.

Current technologies for the measurement of lipid nanotube radii stem from both deterministic and direct measurement approaches. Deterministic approaches, such as tether coalescence[17,18] and electrochemical detection of diffusional species,[19] use a critical physical parameter to determine the size, by measuring the contact angle of coalescence and flow of ions within the nanotube, respectively. Direct measurement by imaging remains a possibility but requires a fast super resolution technique, such as STED, to approach labile species at such short length scales.[21]

These deterministic techniques are entirely complementary, extracting different features depending on their utilization. Coalescence measurements yield external nanotube radii,[17,18] requiring accurate determination of the tube angle and position. Diffusional conductivity measurements estimate the internal radii to be 21−67 nm,[19] requiring electroactive species, which

may be attenuated by strong analyte/membrane interactions. The wide range of current values obtained for lipid nanotube radii is somewhat surprising and is a result of lipid type, composition, lamellarity, and tension variances, difficult to broach with any single technique.

Here we present a new method for the systematic determination of lipid membrane nanotube radii, based on photobleaching and volume expansion of a daughter vesicle (DV), in a minimal two-vesicle nanotube network. This method can be used favorably in platforms utilizing complexes of giant unilamellar vesicles (GUVs) connected to a lipid source, a common configuration used in constructing synthetic networks.[16] Nanotubes are pulled from a vesicle and translocation of the lipid along the nanotube is monitored, during injection and swelling of a DV. This approach is based on fluorescence imaging, deriving the nanotube radii corresponding to the distance from the midpoint in the membrane wall to the center of the nanotube.

Complexes of a multilamellar vesicle (MLV) connected to a giant unilamellar vesicle (GUV) were prepared using a dehydration/rehydration procedure, described elsewhere.[22,23] Briefly, soybean polar lipid extract (SPE) or SPE:chol mixtures (5, 10, and 20 mol %), including membrane dyes, were suspended in chloroform. The solvent was evaporated and then rehydrated using a glycerol containing phosphate buffer. This suspension was left overnight at 4 °C, sonicated, and then aliquoted before freezing. Vesicle samples were prepared by vacuum desiccating a 10 μL droplet, taken from a thawed aliquot, which was placed onto a SU-8 coated #1 coverslip. The resulting film was rehydrated using a phosphate buffer while

situated on the microscope. MLV-GUV complexes formed after several minutes of hydration at room temperature.

The methodology was validated for a known membrane structure using NG-108-15 (NG) cells, where the plasma membrane was made accessible through blebbing.[24,25] Briefly, NG cells were cultured and then transferred to a form-aldehyde−dithiothreitol blebbing solution, containing HEPES and two membrane dyes. This mixture was incubated at 37 °C for 30 min, allowing blebs to form and simultaneously incorporate the fluorescent dyes. The sample was washed with label-free HEPES buffer prior to nanotube formation and analysis.

A nanotube−vesicle network formation procedure was utilized to form nanotubes from MLV−GUV complexes[23] and from plasma membrane blebs.[26] Detailed procedural information for sample preparation, vesicle network generation, and cell manipulation techniques is given in the Supporting Information. Briefly, a pipette pulled from borosilicate glass capillary, used for microelectroinjection, was fitted with a silver electrode and brought into contact with the vesicle membrane using micromanipulators. Using short (6 ms) electrical impulses (60 mV) and contact pressure, the tip of the pipette was inserted through the membrane (Figure 1A). The tip was
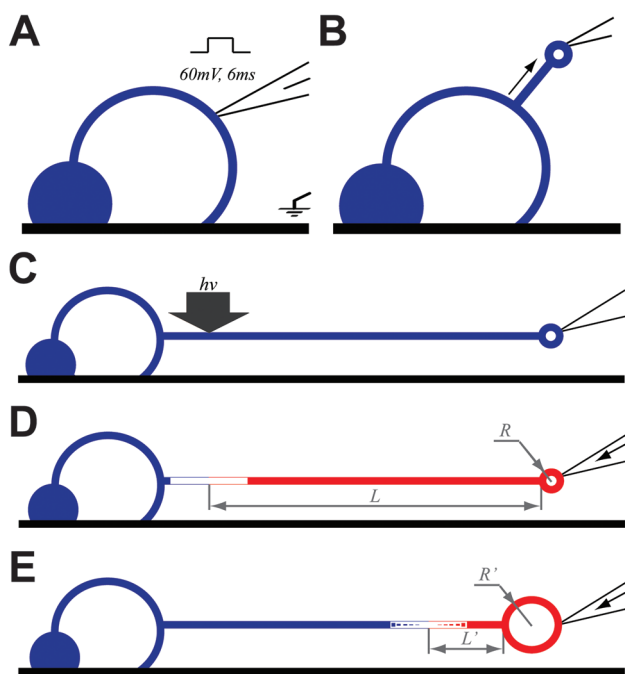

Figure 1. Schematic illustration of the experimental procedure. (A) Electroporation of lipid membrane. (B) Tube generation by translating pipette away from the GUV. (C) Bleaching of the ROI at the beginning of the formed nanotube. (D, E) Slight pressure increase applied to the pipette initiates translocation of the bleached region L−L', coupled with vesicle growth from radius R to R'. The quantity of membrane material on the right-hand side of ROI (red) remains constant.

then withdrawn, bringing with it lipid material, forming a nanotube. Upon application of fluidic pressure to the pipette, a small DV was formed (Figure 1B). When stable, this vesicle was pulled away to a distance of 200−300 μm, thereby forming the nanotube connected vesicle network (Figure 1C). The lipid material provided by the MLV allows for both the nanotube to

elongate and the DV to grow in diameter, with negligible influence on the lateral surface tension, which is essentially maintained over the whole system. Utilizing a confocal microscope (Leica TCS SP2 with a HCX PL APO 40× 1.25 NA oil immersed objective), two channel imaging was performed, $\lambda_{exc/em}$ 488/(500−560) nm and 633/(640−700) nm, to follow the lipid translocation. A ROI on the nanotube was then photobleached in close proximity to the GUV, covering 20−70 μm of total tube length, using all available spectral lines of an Ar⁺ and two HeNe lasers (458, 476, 488, 496, 514, 543, 594, and 633 nm). Upon a slight pressure increase to the DV (Figure 1D), lipid material migrated along the nanotube enabling the DV to grow (Figure 1E). Both movement of the bleached region and the DV growth were imaged at low laser powers and frame rate in an effort to minimize any mitigating photodamage and to maintain signal intensity. For optimal implementation of this technique, a nanotube of 200−300 μm is required along with a DV of initial radius below 5 μm; above this radius, the lipid material translocated along the nanotube is insufficient to detect radial growth. Effects of suboptimal setup are discussed in the Supporting Information. An illustration of an intensity profile measurement can be found in Supporting Information Figure S1.

Nanotube radii were calculated using the surface area conservation law, eq 1, for the growing DV and the nanotube directly following the bleached region (red membrane regions Figure 1D,E)

$$2\pi La + 4\pi R^2 = 2\pi L'a + 4\pi R'^2 \tag{1}$$

where L and L' are the lengths of nanotube from the center of the bleached region to the DV, R is the radius of the DV, and a is the nanotube radius. Surface area of the membrane material to the right of the ROI is conserved for each frame (Figure 2),
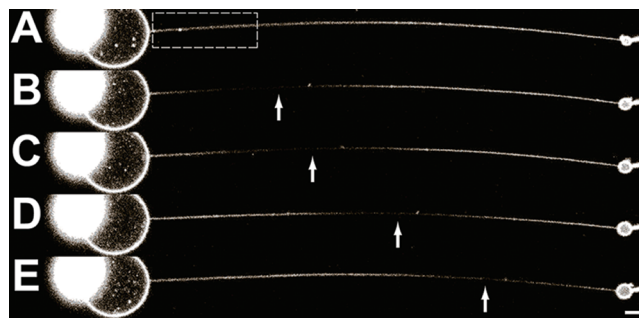

Figure 2. Confocal microscopy images of a typical measurement. (A) A newly created nanotube with the ROI to be bleached highlighted with a dashed line. (B−E) Subsequent time frames at 10, 30, 70, and 110 s show advancement of the bleached region (white arrows) along with the associated DV growth. The scale bar in (E) represents 10 μm.

consisting of nanotube surface area ($2\pi La$) and DV surface area ($4\pi R^2$). The visible portion of the nanotube shortens as a result of lipid material being transferred to the DV during growth.

The equation for nanotube radius determination can be derived from (1) yielding

$$a = 2\Delta R^2/\Delta L \tag{2}$$

where $\Delta L = L − L'$ and $\Delta R^2 = R'^2 − R^2$. From eq 2, nanotube radii can be calculated from the slope of $2\Delta R^2$ plotted against ΔL (Figure 3A).
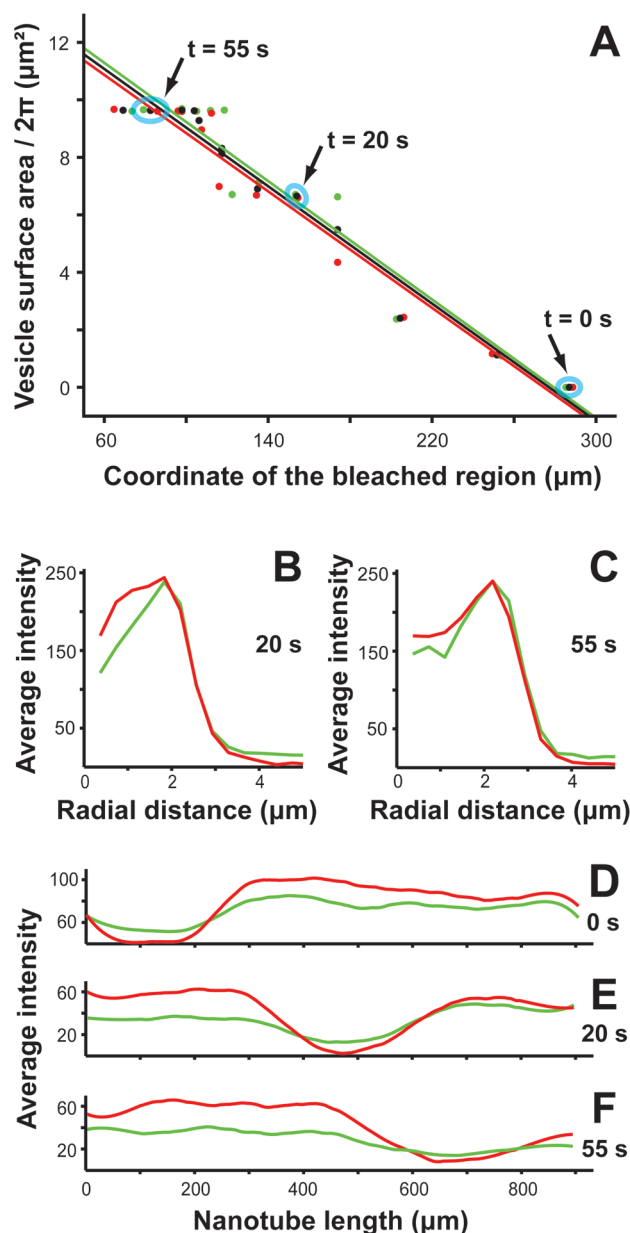
Figure 3. An example of radius determination for SPE plus 10 mol % cholesterol. (A) Changes of DV surface area with translocation of the bleached region are displayed for raw data, with a linear fit presented in green and red for the two fluorophores, along with black representing the mean. Changes in intensity profiles for three time points (blue arrows, A) are illustrated (B−F) for both fluorophores. At $t = 0$ s, the DV within this sequence was no apparent, at the initiation of measurement, resulting in the radius being set to zero. Panels B and C show the intensity distributions used for calculation of the DV radii, illustrated in Figure S1 (C). Intensity profiles along a nanotube (D−F), demonstrating the motion of the bleached region. The final value for the nanotube radius was calculated using an average of the R and L values for both fluorophores, displayed as black dots and fitted with black line in (A). The slope elucidates the tube radius to be 51 nm.

For each MLV−GUV membrane composition analyzed, a minimum of 25 samples (up to 56) were used to construct a representative distribution. Measurement stability was confirmed using two separate control experiments for both small and large diameter DVs (Supporting Information, Figure S3). These controls demonstrated that if a DV does not change in

radius, there is no corresponding translocation of the photobleached ROI along the tube.

A series of images with a translating bleached ROI were recorded for each nanotube (Figure 2), where white arrows denote the ROI. Intensity profiles for both the radius of the growing vesicle "R" (Figure 3B,C) and the coordinate of the bleached region "L" (Figure 3D−F) were used to calculate the nanotube radii. Confocal micrographs were processed in Matlab using custom scripts, further details of which can be found in the Supporting Information (Figure S2). The translation of the ROI was measured for an average of 8 frames, with time intervals of 5−10 s, which was empirically determined to circumvent detrimental diffusional broadening.

It is known that any tension gradient buildup across the nanotube relaxes within milliseconds, but tube radius relaxation takes much longer (few seconds).[27] The MLV−GUV complex connected to the nanotube provides a source of lipid material during the DV expansion, minimizing any tension increase. Equilibrium tension for networks created from SPE MLV−GUV complexes are reported to be on the order of 10^{-6} N/m.[28] In general, lipid membranes can have a very low equilibrium tension $(10^{-9}$ N/m$)$[29] and exhibit transition from an exponential to a linear elasticity regime at tensions between 10^{-4} and 10^{-6} N/m.[29,30] The exponential regime occurs as excess material, hidden within thermal shape fluctuations, becomes consumed and the increased tension smoothes out the membrane. Following this the tension increases linearly as there is a lack of available lipid material. Therefore, if the pressure applied to the DV produces low tension gradients, we can circumvent any tension-related size variation and expect to obtain correct values for the nanotube radii. High tension gradients can affect both the tube radius and lead to shape deformations of the network. When membrane tension increases at a rate exceeding the equilibration rate of the tube radius, a pearling instability can be observed[27] or, alternatively, the DV can migrate freely along the tube.[29] The threshold tension for shape transformation can be represented by

$$\sigma_{\text{pearl}} \sim \frac{\kappa}{r^2} \tag{3}$$

where the bending coefficient $\kappa = 4 \times 10^{-20}$ J[16] is tension independent.[19] If the nanotube is assumed to have a radius of 50 nm, the threshold tension is calculated to be 1.6×10^{-5} N/m, using eq 3.

For accurate radii determination we require any tension increase, arising along the nanotube during experimental manipulation, to be minimal. Tension (σ) was estimated from a force balance (4) of the tension gradient $d\sigma/dx$ and friction drag forces on the tube surface, during membrane transfer:[27]

$$\frac{r \, d\sigma}{dx} = \frac{4\eta V}{\ln\left(\frac{L}{r}\right) - \frac{1}{2}} \tag{4}$$

where r is the nanotube radius, η is the viscosity of water, V is the surface velocity of membrane material, and L is the total tube length. An increase of tension along the tube can be estimated by

$$\Delta\sigma = \frac{4\eta L \Delta L}{r \Delta t \left[\ln\left(\frac{L}{r}\right) - \frac{1}{2}\right]} \tag{5}$$

where $\Delta L = 30$ μm is the progression of the bleached region during time between frames $\Delta t = 10$ s, $L = 200$ μm, and $\eta = 8.9 \times 10^{-4}$ Pa s. The tension along the tube $\Delta\sigma = 5.5 \times 10^{-6}$ N/m, on the same order as the equilibrium tension within SPE networks, placing it in the entropic elasticity regime, allowing us to assume that the obtained results are not sufficiently influenced by the injection procedure.

To accurately map and determine the center of the DV, an average radial intensity plot was constructed, and the membrane location was extracted as the point of maximum intensity (Figure 3B,C). From the DV circumference, the region designating the tube was located and the intensity along its length was measured (Figure 3D−F). As diffusion within the membrane of the nanotube and photodamage of the dyes will blur the edges of the bleached ROI, the positional coordinate for "L" was chosen to be the center of the bleached region, as it is definable, even if the fluorescence intensities decrease. Two membrane dyes were monitored, Bodipy DHPE and "DiD" for vesicle networks or "DiO" and "DiD" for cell plasma membrane blebs, to obtain an average value for R and L, used in the determination of the nanotube radii. By utilizing two independent dye tags, the overall determination accuracy is improved. An example intensity map and determined values for one of the frames from an experimental series are shown in Supporting Information Figure S2.

A histogram plot of the measured nanotube radii was constructed for each SPE membrane composition, incorporating 0−20 mol % cholesterol, using a 1 nm bin (Figure 4). The density function was calculated for each using a moving 5 nm bin and overlaid onto the histogram (Figure 4, blue lines). As the data are from discrete measurements, it was fit using a sum of normal distributions (Figure 4, red lines). The distribution peaks for both SPE and SPE:chol mixtures have standard deviations between 7 and 12 nm, except for the second peak from pure SPE nanotubes, which may have hidden maxima, found using density function analysis with a smaller, 3 nm bin size. The locations of these proposed peak maxima are indicated with black arrows (Figure 4A).

Using the fitted data, we are able to extract the tube radii, which were found to be 40, 65, 80, 91, and 112 nm for pure SPE; 46, 62, and 80 nm for SPE with 5% of cholesterol; 51 and 70 nm for SPE with 10% of cholesterol; and 56, 79, and 99 nm for SPE with 20% of cholesterol. The different radii for each membrane composition are assumed to be representative of the natural distribution of lamellarity of the MLV−GUV complexes. These observed distributions strongly suggest that unilamellar vesicles are 46−60% of the total liposomes generated for SPE:chol mixtures. A similar distribution has been previously observed in analogous systems[31] using fluorometric estimations of the lamellarity.[32] We observed a slightly attenuated distribution of lamellarity for pure SPE membranes, with a lowered percentage of unilamellar vesicles (23%), possibly due to the absence of cholesterol, resulting in a less rigid membrane. This lowered rigidity may allow the vesicles to be more easily destroyed by surface contact wetting, skewing the available population for analysis. Using the same analysis as for the GUV−MLV complexes, NG membrane blebs result in a single distribution, wider than any single lamellar distribution measured from vesicles (Supporting Information Figure S7). The density functions were fitted, obtaining a peak at 69 nm with a standard deviation of 18 nm. Several values were measured at significantly lower radii than the peak, likely due to a limitation of material leading to an overstretching of
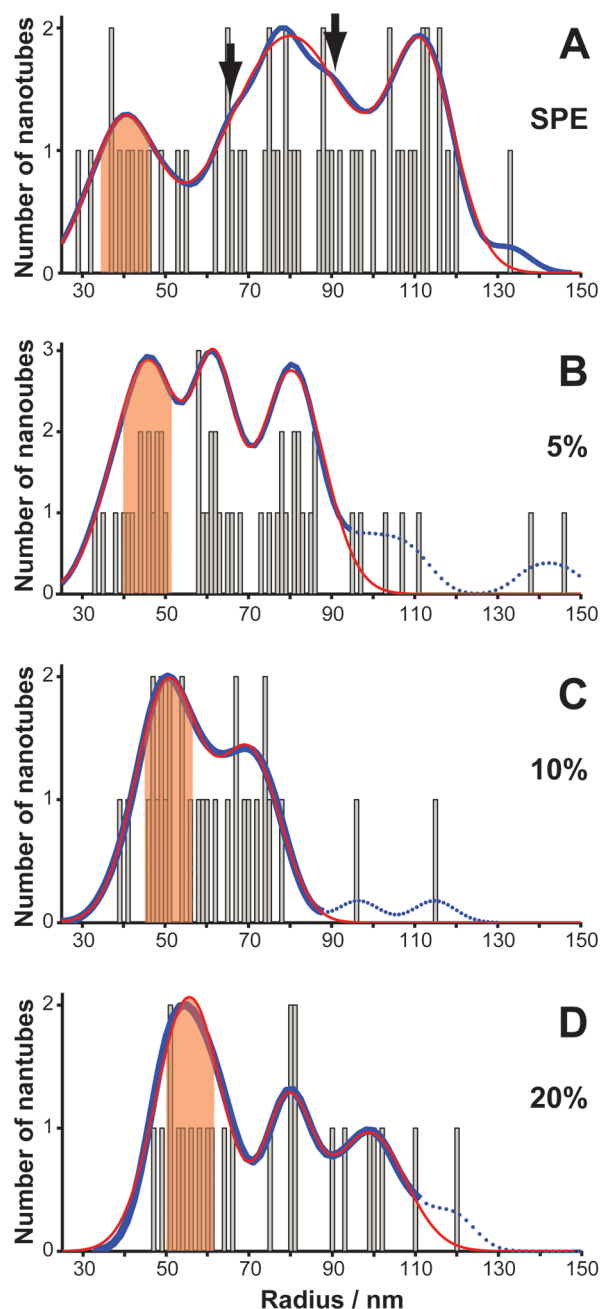

Figure 4. Results of the nanotube radii obtained for different membrane compositions. Histograms were constructed using a 1 nm bin (gray) for nanotubes formed from different membrane compositions: (A) SPE; (B−D) SPE with addition of 5, 10, and 20 mol % of cholesterol. These histograms are overlaid with density function plots calculated using a moving 5 nm bin (blue line). The solid blue line represents the part of the density functions that were used to fit a sum of normal distributions (red line). Broken blue lines represent part of the density functions that were not fit due to low numbers of data points at these radial sizes. The fitted peaks have standard deviations of 7−12 nm, except for the second peak of pure SPE, which may have hidden maxima found from the density function analysis with a smaller 3 nm bin size (black arrows indicate possible peak maxima locations).

the membrane. Cell plasma membrane nanotubes are certainly unilamellar and the peak position suggests that plasma membrane are more rigid then SPE containing 20 mol% cholesterol.

It is assumed that the degree of lamellarity for all created network elements remains the same, as all lamellae should be held by pipette, or retracted to the original vesicle. The lamellarity of the vesicle network elements measured does not influence the measurement strategy for nanotube radii determination (2), as values of R are derived from fluorescence images. The membrane can be seen as a point emitter (due to the thickness being below the optical resolution), the intensity maxima will therefore map to the midpoint in the membrane. The position of this membrane midpoint is displayed in Figure 5A−C for uni-, bi-, and trilamellar vesicles. The nanotube radii
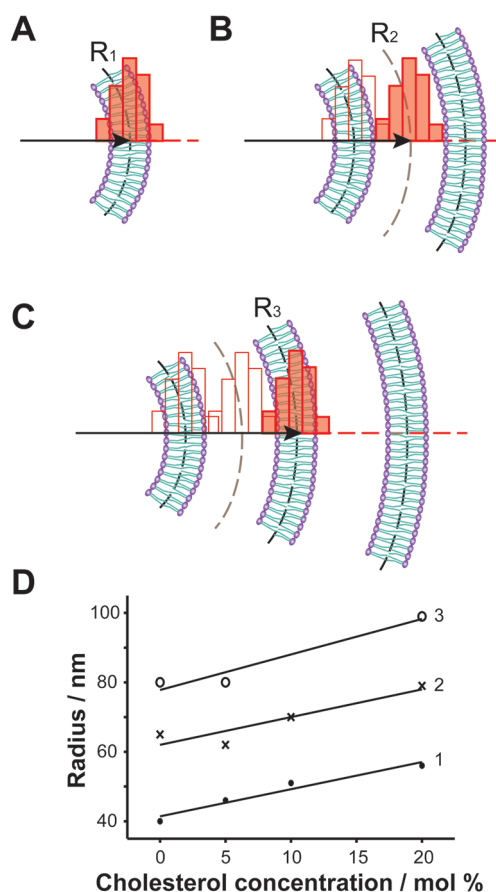

Figure 5. Illustration of the origin for the measured value of radii distributions (shown in red) for nanotubes of one (A), two (B), and three (C) lamellae. Nanotube radii dependence upon cholesterol concentration is highlighted in (D) for 1 (●), 2 (×), and 3 (○) lamellar nanotubes, indicating measurable compositional changes.

we measured are therefore the distance from the center of the nanotube to the midpoint in the membrane lamellae.

It should be noted that the distance between the peaks (11−25 nm) is equal to half the distance between the lamellae, the origins of which are illustrated in Figure 5A−C. This assumes that the inner lamella of the membranes has the same curvature, independent of the total number of lamellae. The distance between the centers of the lamellae is therefore 22−50 nm, which is of the same order as 24−25 nm measured for ionic surfactants[33] and with 70−130 nm using microemulsion systems.[34]

The SPE unilamellar tube radius of 40 nm closely matches the nanotubes, inner radius, obtained by electrochemical measurement of the flow of catechols, 23−57 nm.[19] The

average radius of SPE nanotubes from our results is 80 nm, which from the distribution plot (Figure 4A) corresponds to trilamellar nanotubes. The external radii for a trilamellar nanotube would be increased by the thickness of the separation between the lamellae (22−41 nm for SPE membrane from Figure 4A), making it equivalent to an outer radii of 102−121 nm. This agrees very well the value of 110 nm obtained for SPE nanotubes when using the tether coalescence method.[17]

Cholesterol, being a naturally occurring component of the cell membrane, is known to increase both bending rigidity and the elastic area compressibility modulus of the membrane.[30] Determination of the cholesterol content has particular current interest, with links to immunological function, as inhibition of cholesterol biosynthesis has been shown to interfere with intracellular trafficking of liposomes in antigen processing pathways;[35] neurological function, as cholesterol distribution between synaptic plasma membrane leaflets can be modified by different conditions in vivo, such as chronic ethanol consumption, statins or aging;[36] and diseases, as cholesterol transport processes may be altered in Alzheimer's disease.[37] Compositional cholesterol variances are also correlated with adaption as a result of environmental stimuli.[38]

Our approach demonstrated sensitivity sufficient to detect the influence of cholesterol on nanotube radii (Figure 5D). Based upon the calculated distributions for uni-, bi-, and trilamellar nanotubes, respectively, there is a trend of increasing radii with increasing levels of cholesterol. It is well established that addition of cholesterol leads to higher membrane rigidity, opposing membrane bending, which should result in an increase of radius. The radius of a lipid nanotube in an equilibrium state can be calculated from a balance of the bending and tension forces:

$$r = \left(\frac{\kappa}{2\sigma}\right)^{1/2} \tag{6}$$

where the bending coefficient κ has been reported to increase with cholesterol concentration for SOPC membranes.[30] By augmenting the membrane to 50 mol % of cholesterol, κ can increase 2−3 times.[39] Assuming that the equilibrium tension does not change with addition of cholesterol, the bending coefficient for unilamellar vesicles, calculated from the measured radii, will increase in 1.3, 1.6, and 2 times, with addition of 5, 10, and 20 mol % of cholesterol, respectively. This range being biologically relevant, as the typical total cholesterol content found within mammalian cell membranes is 20−30 mol %.[40]

To interrogate cell membrane composition, plasma membrane blebs must first be generated, to release the lipid material from the cytoskeleton. This was investigated using NG cells, as they have been previously documented as having readily available membrane material, a prerequisite in creating both a long nanotube and a sufficiently sized DV (Supporting Information, Figure S6).[26] Tension can be introduced into the network, if the easily accessible lipid material, is insufficient to support the growth of the DV. This was experimentally observed for some membrane blebs, as they retained a weak connection to the cell, limiting the material supply and causing a prompt tension increase, resulting in a narrowing of the tube radius. This same effect has been seen in nanotubes pulled from Egg PC GUVs, without a MLV reservoir, leading to a tube radii estimation of 10−40 nm.[18]

We cannot directly compare radii values between vesicle networks and cell blebs, as cell membranes contain numerous additional components, whose influence we cannot readily predict. One example of such an inclusion being 0.05 mol % of short peptides (16−24 amino acids) in SOPS:chol (3:2) and in DMPC:chol (3:2) mixtures results in measurable differences of the elastic area compressibility modulus.[41]

Error estimations were made on the vesicle networks through sequential analysis on the same nanotubes, scrutinizing the measurement variance. An average of four measurements for each of three nanotubes pulled from different SPE vesicles (Supporting Information, Figure S4) resulted in mean values of 32, 46, and 37 nm, with standard deviations of 10, 18, and 6 nm. The obtained values are within the expected range for the first "unilamellar" peak of the SPE distribution, with standard deviations closely matching the widths of normal distribution fitted to all the peaks, implying our measurement is reproducible within experimental bounds.

The major contributors to the measurement uncertainty can be classified by three sources of error: imaging focal plane shift from middle plane of the DV, uncertainty of DV radius determination, and uncertainty of bleached region coordinate determination. A detailed breakdown of their effects is given in the Supporting Information. The leading cause of uncertainty was found to be in the determination of DV radius, having variances on the same order as the experimentally measured standard deviations. Using DVs with a larger R can decrease relative uncertainty, there is however a sensitive balance between "R" and "ΔR" measurements. It is necessary to form R large enough for ease of determination, while maintaining a measurable ΔR, through incorporation of 250−300 μm nanotube material. R was calculated to have an upper limit of 5 μm, above which ΔR becomes too small to measure (optimal technique employment, Supporting Information). Using larger vesicles would require a larger field of view to accommodate longer nanotubes to provide enough material for a sufficient ΔR.

In comparison with other deterministic approaches, an accurate measurement of the tube angle and position is not required, nor is introduction of electroactive analytes within the network, lowering the dependence on positional fluctuations and influence of solute membrane interactions. A direct imaging technique as STED could be employed to measure an average value of the nanotube width but would be at the bounds of its optical resolution for standard implementation, which is typically 65 nm.[42,43] This approach requires highly specialized microscopy, specifically photostable dyes, and would be difficult to measure smaller scale nanotubes or minor size fluctuations without extensive interpolation. In addition to the clear benefits in characterization of nanotube−vesicle networks, the method is also well suited to determining compositional variances of cell membranes.

In conclusion, we have successfully measured nanotube radii without many of the experiment constraints of previous schemes (positioning and electroactive species flow), while able to make attributions to lamellarity and membrane composition. We have validated analysis sensitivity through the modulation of membrane cholesterol concentration from 0 to 20%, measuring the effect on nanotube radius and subsequent membrane rigidity. Method ubiquity was demonstrated using NG-108-15 cells, resulting in measured tube radii of 69 nm, further indicating the possibility for measuring cell membrane compositional variances.

■ ASSOCIATED CONTENT

ⓢ Supporting Information

Additional information on materials and methods, image processing in Matlab, the origins of measurement error, and the application to cell plasma membrane nanotubes. This material is available free of charge via the Internet at http://pubs.acs.org.

■ AUTHOR INFORMATION

Corresponding Author

*Tel +46 31-772 6112; fax +46 31-772 2750; e-mail aldo@chalmers.se.

Notes

The authors declare no competing financial interest.

■ ACKNOWLEDGMENTS

■ REFERENCES

(1) Lippincott-Schwartz, J.; Donaldson, J. G.; Schweizer, A.; Berger, E. G.; Hauri, H. P.; Yuan, L. C.; Klausner, R. D. *Cell* **1990**, *60*, 821.

(2) Lippincott-Schwartz, J.; Yuan, L.; Tipper, C.; Amherdt, M.; Orci, L.; Klausner, R. D. *Cell* **1991**, *67*, 601.

(3) Chiu, D. T.; Hurtig, J.; Onfelt, B. *Wires Nanomed. Nanobi.* **2010**, *2*, 260.

(4) Rustom, A.; Saffrich, R.; Markovic, I.; Walther, P.; Gerdes, H. H. *Science* **2004**, *303* (5660), 1007.

(5) Carlin, L. M.; Eleme, K.; McCann, F. E.; Davis, D. M. *J. Exp. Med.* **2001**, *194*, 1507.

(6) McCann, F. E.; Eissmann, P.; Önfelt, B.; Leung, R.; Davis, D. M. *J. Immunol.* **2007**, *178*, 3418.

(7) Vanherberghen, B.; Andersson, K.; Carlin, L. M.; Nolte-'t Hoen, E. N.; Williams, G. S.; Hoglund, P.; Davis, D. M. *Proc. Natl. Acad. Sci. U. S. A.* **2004**, *101*, 16873.

(8) Gousset, K.; Schiff, E.; Langevin, C.; Marijanovic, Z.; Caputo, A.; Browman, D. T.; Chenouard, N.; de Chaumont, F.; Martino, A.; Enninga, J.; Olivo-Marin, J. C.; Mannel, D.; Zurzolo, C. *Nat. Cell Biol.* **2009**, *11*, 328.

(9) Lehmann, M. J.; Sherer, N. M.; Marks, C. B.; Pypaert, M.; Mothes, W. *J. Cell Biol.* **2005**, *170*, 317.

(10) Magalhaes, A. C.; Baron, G. S.; Lee, K. S.; Steele-Mortimer, O.; Dorward, D.; Prado, M. A.; Caughey, B. *J. Neurosci.* **2005**, *25*, 5207.

(11) Onfelt, B.; Nedvetzki, S.; Benninger, R. K.; Purbhoo, M. A.; Sowinski, S.; Hume, A. N.; Seabra, M. C.; Neil, M. A.; French, P. M.; Davis, D. M. *J. Immunol.* **2006**, *177*, 8476.

(12) Sowinski, S.; Jolly, C; Berninghausen, O.; Purbhoo, M. A.; Chauveau, A.; Jolly, C.; Berninghausen, O.; Purbhoo, M. A.; Chauveau, A.; Kohler, K.; Oddos, S.; Eissmann, P.; Brodsky, F. M.; Hopkins, C.; Onfelt, B.; Sattentau, Q.; Davis, D. M. *Nat. Cell Biol.* **2008**, *10*, 211.

(13) Watkins, S. C.; Salter, R. D. *Immunity* **2005**, *23*, 309.

(14) Obermajer, N.; Jevnikar, Z.; Doljak, B.; Sadaghiani, A. M.; Bogyo, M.; Kos, J. *Cell. Mol. Life Sci.* **2009**, *66*, 1126.

(15) Sherer, N. M.; Lehmann, M. J.; Jimenez-Soto, L. F.; Horensavitz, C.; Pypaert, M.; Mothes, W. *Nat. Cell Biol.* **2007**, *9*, 310.

(16) Jesorka, A.; Orwar, O. *Annu. Rev. Anal. Chem.* **2008**, *1*, 801.

(17) Akerman, B.; Tokarz, M.; Hakonen, B.; Dommersnes, P.; Orwar, O. *Langmuir* **2007**, *23*, 7652.

(18) Cuvelier, D.; I, D.; Bassereau, P.; Nassoy, P. *Biophys. J.* **2005**, *88*, 2714.

(19) Adams, K. L.; Engelbrektsson, J.; Voinova, M.; Zhang, B.; Eves, D. J.; Karlsson, R.; Heien, M. L.; Cans, A. S.; Ewing, A. G. *Anal. Chem.* **2010**, *82*, 1020.

(20) Abbe, E. *Proc. Bristol Naturalists' Soc.* **1874**, *1*, 200.

(21) Willig, K. I.; Keller, J.; Bossi, M.; Hell, S. W. *New J. Phys.* **2006**, *8*, xxxx.

(22) Criado, M.; Keller, B. U. *FEBS Lett.* **1987**, *224*, 172.

(23) Karlsson, M.; Sott, K.; Cans, A. S.; Karlsson, A.; Karlsson, R.; Orwar, O. *Langmuir* **2001**, *17*, 6754.

(24) Holowka, D.; Baird, B. *J. Biol. Chem.* **1984**, *259*, 3720.

(25) Baumann, N. A.; Vidugiriene, J.; Machamer, C. E.; Menon, A. K. *J. Biol. Chem.* **2000**, *275*, 7378.

(26) Bauer, B.; Davidson, M.; Orwar, O. *Langmuir* **2006**, *22*, 9329.

(27) Dommersnes, P. G.; Orwar, O.; Brochard-Wyart, F.; Joanny, J. F. *Europhys. Lett.* **2005**, *70*, 271.

(28) Lobovkina, T.; Dommersnes, P.; Joanny, J. F.; Hurtig, J.; Orwar, O. *Phys. Rev. Lett.* **2006**, *97*, 188105.

(29) Bar-Ziv, R.; Moses, E.; Nelson, P. *Biophys. J.* **1998**, *75*, 294.

(30) Evans, E.; Rawicz, W. *Phys. Rev. Lett.* **1990**, *64*, 2094.

(31) Billerit, C.; Wegrzyn, I.; Jeffries, G. D. M.; Dommersnes, P.; Orwar, O.; Jesorka, A. *Soft Matter* **2011**, *7*, 9751.

(32) Akashi, K.; Miyata, H.; Itoh, H.; Kinosita, K. Jr. *Biophys. J.* **1996**, *71*, 3242.

(33) Soubiran, L.; Coulon, C.; Sierro, P.; Roux, D. *Europhys. Lett.* **1995**, *31*, 243.

(34) Strey, R.; Jahn, W.; Porte, G.; Bassereau, P. *Langmuir* **1990**, *6*, 1635.

(35) Rao, M.; Peachman, K. K.; Alving, C. R.; Rothwell, S. W. *Immunol. Cell Biol.* **2003**, *81*, 415.

(36) Wood, W. G.; Igbavboa, U.; Muller, W. E.; Eckert, G. P. *J. Neurochem.* **2011**, *116*, 684.

(37) Knebl, J.; DeFazio, P.; Clearfield, M. B.; Little, L.; McConathy, W. J.; McPherson, R.; Lacko, A. G. *Mech. Ageing Dev.* **1994**, *73*, 69.

(38) Hazel, J. R.; Williams, E. E. *Prog. Lipid Res.* **1990**, *29*, 167.

(39) Hochmuth, R. M.; Shao, J. Y.; Dai, J. W.; Sheetz, M. P. *Biophys. J.* **1996**, *70*, 358.

(40) Rog, T.; Pasenkiewicz-Gierula, M.; Vattulainen, I.; Karttunen, M. *Biochim. Biophys. Acta* **2009**, *1788*, 97.

(41) Evans, E.; Needham, D. *Faraday Discuss.* **1986**, *81*, 267.

(42) Willig, K. I.; Stiel, A. C.; Brakemann, T.; Jakobs, S.; Hell, S. W. *Nano Lett.* **2011**, *11*, 3970.

(43) Hell, S. W.; Wichmann, J. *Opt. Lett.* **1994**, *19*, 780.